Protection and Control of
Modern Power Systems

ORIGINAL RESEARCH   **Open Access**

Fault-line selection and fault-type recognition in DC systems based on graph theory

Yan Xu, Jingyan Liu[*] and Yuan Fu

Abstract

When a fault occurs in a DC system, the fault current rises rapidly with no zero-crossing point which makes fault-line selection and fault-type identification difficult. In this paper, an online detection and protection method based on graph theory, namely the "double *D* method", is proposed for fault-line selection and fault-type identification in DC systems. In the proposed method, the entire distribution network is visualized as a "map" with vertices representing the line convergence points and edges representing the connection lines. A network topology matrix "*D*" is formed by detecting the current directions as the current directions are altered following a fault, whereas the current directions at the ends of non-fault lines remain the same. In order to prevent misjudgment problems arising from power flow reversal, the rates of change of the fault currents are used to further determine whether a fault has occurred and the "double *D* method" is introduced to identify the fault type. Simulations results with different fault types verify the effectiveness and reliability of the proposed method.

Keywords: Network topology matrix, Double *D* method, Fault-line selection, Fault-type identification, Graph theory

1 Introduction

When large amount of renewable energy is connected to a traditional power grid, it becomes increasingly difficult for the grid to handle problems such as grid stability. Therefore, it is necessary to upgrade the traditional technologies. DC power systems have recently attracted significant attentions owing to their advantages such as high flexibility, controllability of power and improving power angle stability [1]. In city distribution networks, DC loads such as electric cars and lighting systems are developing and expanding rapidly. In view of this, the construction of DC distribution networks can not only reduce the number of power conversion links but also improve the power supply efficiency. In general, voltage-source converters (VSC) can have the two-level, three-level, or modular multilevel converter (MMC) topologies. The modulation principles of the two-level and three-level converters are the same, whereas two-level converters with the advantages of mature technology, simple control, and a low cost, have greater application prospects than MMC in

distribution networks. Faults occurred in a DC line within a VSC based multi-terminal DC distribution network will have wider influences on the whole system than in a two-terminal DC transmission system. Therefore, to maintain safe operation, it is of great importance to study the fault-selection and fault-type recognition methods for DC lines to detect and remove the fault quickly.

Two main methods are used for fault location in DC power grids, i.e. the traveling wave method and the fault analysis method [2, 3]. Considering the similar physical natures of AC and DC lines, most studies have focused on application of fault location principles of AC lines to DC lines. The current fault location methods used in DC line fault location devices in commercial operations still predominantly use the traveling wave method [4–9]. By using the difference in the transmission time between the fault position and measuring point detected by the transient traveling wave, the fault location can be obtained. This method is not influenced by the type of line, fault impedance, fault type or system parameters on either side and thus has a relatively high location precision [10–12]. However, some technical problems that are difficult to overcome still exist. The identification

* Correspondence: m18330215502_1@163.com
State Key Laboratory of New Energy and Electric Power Systems, North China Electric Power University, Baoding 071003, Hebei, China

Xu et al. Protection and Control of Modern Power Systems (2018) 3:27

Page 2 of 10

and calibration of the wave head are highly dependent on the competence of the operating persons and therefore, it is difficult to realize automation. Moreover, the traveling wave fault location system requires a high sampling rate to accurately control the positioning error to within a certain range. With a limited wave amplitude, it is difficult to calibrate the starting point of the wave head accurately which can result in inaccurate fault location.

To solve the problems listed above, reference [13] proposed a fault location method for a DC line based on non-traveling wave principle using the electrical quantities of a single terminal to realize fault location. In theory, the amount of calculations required is relatively small and the results have good accuracy. However, it is prone to converter regulation on the opposite side. Moreover, the method was set up based on the hypothesis that the fault currents of the DC lines are provided by the rectifier alone, which is not true in practical systems. Reference [14] proposed a non-traveling wave principle and a fault location method of DC lines using only the electrical quantities of a single terminal. The advantages of this method, such as the relatively low requirements on sampling rate and minimal influence of transition resistance are attractive. However, the calculation process is rather complex resulting in unsatisfactory location accuracy in practical applications. A fault location principle for high-voltage direct current (HVDC) transmission lines was proposed in [15] using the natural frequency of the current. Using the electrical quantities of only a single terminal, it realized fault location with high speed and accuracy but required a system with high sampling frequency.

In this study, the DC-fault transient processes of DC power distribution systems are analyzed. Methods of fault-line selection and fault-type identification in a DC system are proposed based on graph theory. Fault-line selection is mainly accomplished by the combination of judging the current flow and extracting the di/dt fault feature.

2 Discussion
2.1 Analysis of DC line fault
2.1.1 Distribution network topology
The topology of a DC power distribution system can be classified into parallel type and tandem type. The parallel type can be further divided into ring connections and tree connections [10]. The tandem topology, and the ring and tree connection topologies are shown in Fig. 1, and Fig. 2a and b, respectively [11]. The DC voltage at each end of the converter station in a parallel system is the same and power distribution is achieved by changing the DC current at each end. In contrast, in the tandem system, the converter stations operate with the same DC current and power
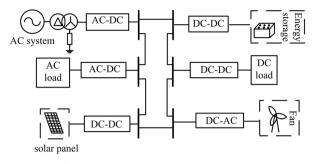

Fig. 1 Tandem type

distribution is achieved by changing the DC voltages. When compared with the tandem system, the parallel system has the advantages of lower line loss, wider adjustment range, easier expansion, etc. For a multi-terminal flexible DC system, the system connection is generally in parallel to ensure that the converters operate at the same DC voltage level.

The system diagram when a pole-to-pole fault occurs in a DC system is shown in Fig. 3. The whole fault process is divided into the DC capacitor discharge stage, diode freewheeling stage and steady-state AC power stage [14]. If the DC-side capacitor voltage drops to zero during a DC short-circuit fault, it will behave like a three-phase short circuit on the AC side and lead to a rapid overcurrent on the freewheeling diodes which can
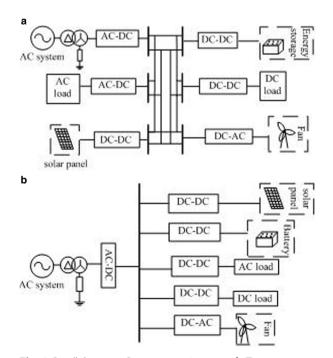

Fig. 2 Parallel type. **a** Ring connection type. **b** Tree connection type
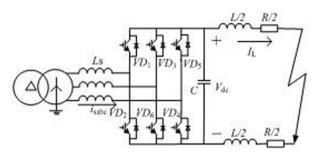
Fig. 3 System diagram for pole-to-pole faults

seriously affect the safe operation of the AC system and damage the freewheeling diodes. Therefore, in order to fully protect the DC lines, inverters and AC systems, a quick protection action and DC circuit breaker tripping should occur before the DC capacitor voltage discharges to zero. This prevents a three-phase short circuit condition on the AC side and large diode overcurrent. Therefore, this study mainly focuses on the capacitor discharge stage [16].
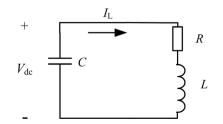
2.2 Analysis of pole-to-pole fault

During the initial fault stage, the insulated gate bipolar transistor (IGBT) can be quickly blocked and the current from the AC side is negligible. Thus, the current on the DC line comes from the discharge of the capacitor and the equivalent circuit is shown in Fig. 4 [17].

In Fig. 3, C is the DC capacitance, V_{dc} is the capacitor voltage, R is the line resistance, L is the line inductance and I_L is the current flowing through the line. $VD_i(i = 1,2,...6)$ denotes an insulated gate bipolar transistor in a circulating bridge. L_s represents the AC side inductance. I_{sabc} indicates the current flowing through the inductor on the AC side.

According to the Kirchhoff Voltage Law (KVL), there is

$$LC\frac{d^2 V_{dc}}{dt^2} + RC\frac{dV_{dc}}{dt} + V_{dc} = 0 \tag{1}$$

It assumes that the DC system has a short-circuit fault at time t_0, the initial values of the voltage and current are assumed to be V_0 and I_0, respectively. The line resistance is usually small and thus, $R < 2\sqrt{L/C}$. Solving (1) gives the transient expressions for the voltage V_{dc} and current I_L as

$$V_{dc} = \frac{V_0\omega_0}{\omega}e^{-\delta t}\sin(\omega t + \beta) - \frac{I_0}{\omega C}e\,\sin(\omega t) \tag{2}$$

$$I_L = C\frac{dV_{dc}}{dt} = \frac{I_0\omega_0}{\omega}e^{-\delta t}\sin(\omega t - \beta) + \frac{V_0}{\omega L}e^{-\delta t}\sin(\omega t) \tag{3}$$

where

$$\begin{cases} \omega_0 = \sqrt{\delta^2 + \omega^2} = 1/\sqrt{LC} \\ \beta = \arctan(\omega/\delta) \\ \delta = R/2L \\ \omega^2 = 1/LC - (R/2L)^2 \end{cases} \tag{4}$$

2.3 Analysis of pole-to-ground fault

The equivalent circuit of the capacitor discharge phase when a pole-to-ground fault occurs in a DC power distribution system is shown in Fig. 5 [18].

The fault process starts from the DC-side capacitor discharge. The DC capacitor, fault line and ground impedance form a second-order discharge circuit. After fault occurrence, the capacitor begins to discharge through this circuit. The equivalent circuit is shown in Fig. 6.

According to KVL, there is

$$LC\frac{d^2 V_{dc}}{dt^2} + (R + R_f)C\frac{dV_{dc}}{dt} + V_{dc} = 0 \tag{5}$$
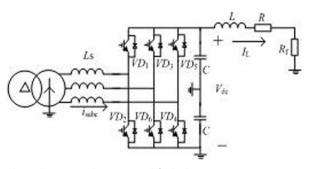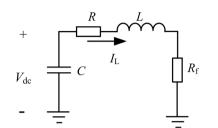
where R_f is the grounding resistance.

Fig. 4 Equivalent circuit diagram of capacitance discharge phase under pole-to-pole fault

Fig. 5 Positive pole-to-ground fault diagram

Xu et al. Protection and Control of Modern Power Systems (2018) 3:27

Page 4 of 10

Fig. 6 Equivalent circuit diagram of capacitance discharge in pole-to-ground fault

After the fault occurs, the process can be treated as a zero-input response. Under normal circumstances, the line resistance and grounding resistance are relatively small and therefore, the system meets the under-damping condition of $R + R_f < 2\sqrt{L/C}$. Thus, the DC voltage and current are given as

$$V_{dc} = e^{at}(C_1 \cos bt + C_2 \sin bt) \qquad (6)$$

$$I_L = -C\frac{dV_{dc}}{dt} = -Ce^{at}[(C_2A - C_1B)\sin bt + (C_1A + C_2B)\cos bt] \qquad (7)$$

where

$$\begin{cases} a = -\dfrac{R + R_f}{2L} \\ b = \sqrt{\dfrac{1}{LC} - \left(\dfrac{R + R_f}{2L}\right)^2} \\ C_1 = U_0 \\ C_2 = \dfrac{(R + R_f)U_0C - 2LI_0}{\sqrt{4LC - (R + R_f)^2 C^2}} \end{cases} \qquad (8)$$

3 Methods
3.1 Fault-line selection based on graph theory
3.1.1 Basics of graph theory
Definition 1: A graph consists of several different vertices and edges connecting the different vertices [19].

The constituent elements of a graph are the points which are often called vertices, and the edges which are ordered pairs of vertices. If two vertices can be connected by an edge, the two have adjacent relations. The chart can generally be shown as $G = (V, E)$, where $V = [v_1, v_2, ..., v_n]$ is the collection of all vertices, and $E = [e_1, e_2, ..., e_n]$ is a multiple subset of the Cartesian product whose elements are directed edges and are simply called edges.

Definition 2: Suppose $G = (V, E)$ is a digraph with no margin. When $V = [v_1, v_2, ..., v_n]$, the N × N matrix $D = [d_{ij}]$ is called the adjacency matrix of the **G** graph, denoted as **D[G]**. The adjacency matrix is a matrix representing the relationship between the vertices as

$$d_{ij} = \begin{cases} 0\,(v_i, v_j) \notin E \\ 1\,(v_i, v_j) \in E \end{cases} \qquad (9)$$

3.2 Directed topology description of distribution network
Irrespective of the type of the network structure, the system is composed of switches, overhead lines and a variety of other devices. Thus, the network composition can be simplified and the directional topology of the distribution network can be obtained.

According to Definition 1, the intersection of the distribution network lines can be seen as a vertex and the feeder between two adjacent vertices as an edge. Thus, the distribution network can be seen as a map. The connection relationship between the vertex and feeder in the distribution network can be described by the definition of the graph, and the topology of the distribution network can be described by the adjacency matrix in Definition 2.

When a fault occurs, the direction of the current flowing through the distribution feeder will change suddenly. Therefore, the feeder of the distribution network can be viewed as a directional edge. Assuming that the number of nodes in the distribution network is n, the distribution network (hereafter referred to as the network topology matrix) can be described by an n-order adjacency matrix **D**. If the direction of the edge is vertex i pointing to vertex j, the element $d_{ij} = 1$ in matrix **D**. If the direction of the edge is vertex j pointing to vertex i, the element $d_{ij} = -1$ in matrix **D**. The remaining elements are all zero and the end nodes are all set to zero. That is, the positive direction of each current transformer is defined as the vertex pointing to the line.

In actual applications, the judgment of the current direction can be obtained by matching the current transformer and the ammeter. The connection method is shown in Fig. 7. As shown, the primary coil has a leading end L_1 and a trailing end L_2. The first end of the secondary coil is K_1 and the other end is K_2. The positive direction of the ammeter is indicated by the black arrow in Fig. 7a and "*" indicates the same polarity of the current transformer.

Figure 7a shows the current flow in the current transformer under normal system operation. As there is no significant change in the primary current, no current is induced on the secondary side and the ammeter does not register any current. The element in matrix **D** is thus

Xu *et al. Protection and Control of Modern Power Systems* (2018) 3:27
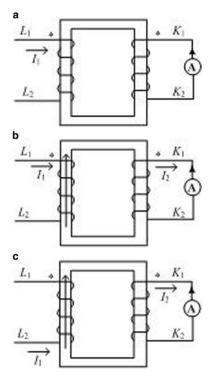
Page 5 of 10

Fig. 7 Current direction acquisition diagram. **a** Normal operation. **b** l1 decreases rapidly. **c** l1 increases rapidly

"1" at this time. When the current at the detection point changes, the primary current of the current transformer undergoes two processes. Firstly, the flow of I_1 from the L_1terminal rapidly decreases to zero. Then, the direction of I_1 changes and the current flows from the L_2 terminal rapidly increases. The direction of the current induced on the secondary side shown in Fig. 7b and c, is opposite to the positive direction of the current meter and the sign of the current flowing through the current meter is thus negative. At this time, the element in matrix D is "– 1."

3.3 Matrix fault criterion and fault detection
For a system under normal operation, current transformers are added at both ends of each line. The positive direction of the current transformer is defined as the direction pointing from the apex to the line. Therefore, the distribution of elements in matrix D in normal operation will be symmetrical, and the values in the symmetrical positions will be "1" and "– 1." In case of a fault, the current directions of the non-faulty lines will be consistent with the above description and the current directions of the faulty lines will be the same as the specified positive direction. Assuming that the vertices at either end of the faulty line are a and b, in matrix

D, $d_{ab} = d_{ba} = 1$. The fault information matrix S is introduced as $s_{ij} = d_{ij} + d_{ji}$ and the fault criterion is given as

$$s_{ij} = \begin{cases} = 0 \text{ The line between } i \text{ and } j \text{ is working properly} \\ \neq 0 \ \text{ The line between } i \text{ and } j \text{ has failed} \end{cases}$$

$$(i = 1, 2, ...n \ ; j > i)$$

$$(10)$$

where n represents the number of vertices.

When the system is in normal operation, all the elements in the S matrix will be 0. When a fault occurs, the elements in the faulty line will be 2 while the remaining elements will be 0. The fault information matrix can show whether the system is faulty and determine the location of the faulty line.

The proposed method based on graph theory forms a network topology matrix. When the logical elements are determined, the running states are represented by 0, 1 and – 1. The matrix generation speed is fast, the sparseness is strong and the operation speed is also fast.

3.4 Shortcomings and improvements of the proposed method
3.4.1 Preventing misjudgment and extracting the degree of failure di/dt
When the power flow of the system changes during normal operation, using the abovementioned algorithm alone may result in misjudgment. di/dt is commonly used to characterize the current characteristics of different locations. The current change rates of the branches under pole-to-pole fault and pole-to-ground fault conditions can be calculated using (3) and (7), respectively. However, they only consider the effects of single-terminal systems and ignore the effects of others in the multi-terminal system on the fault current. Due to the inhibitory effect between shunt capacitors, the more terminals there are the smaller the fault current is. However, the fault current in a multi-terminal system will not be less than 1/2 of that under single-ended operation, Therefore, in order to avoid the influence of power-flow reversal, it is assumed that only the converter station closest to the fault point is operational when calculating the current setting value. If the set value of the fault-current change rate is b_{kc}, the additional fault criterion is

$$\frac{di}{dt} \geq \frac{1}{2} b_{kc} \quad\quad\quad (11)$$

Through the current transformer, the current value of every moment can be collected and the current change rate di/dt is calculated by the difference method. As long as the sampling time interval is properly controlled, the positioning accuracy can be guaranteed. The sampling interval can be selected from 20 to 100 μs depending on the transient characteristics of the DC system. The value of di/dt at time

Xu *et al. Protection and Control of Modern Power Systems* (2018) 3:27

Page 6 of 10

t_c can be approximated using the backward difference method as

$$\frac{\mathrm{d}i}{\mathrm{d}t} = \lim_{\Delta t \to 0} \frac{i(t_c + \Delta t) - i(t_c)}{\Delta t} \approx \frac{\Delta i}{\Delta t} \\ = \frac{i(k) - i(k-1)}{\Delta t} \tag{12}$$

where k is the sampling instant, $i(k)$ and $i(k-1)$ are the sampled currents at the kth and $(k\text{-}1)^{\mathrm{th}}$ instants, respectively, and Δt is the sampling interval.

When S is an all-zero matrix, it is not necessary to use (11) because the change of the current direction is a necessary and insufficient condition for fault occurrence. When S is a non-all-zero matrix, the line corresponding to the non-all-zero elements is confirmed first, and the $\mathrm{d}i/\mathrm{d}t$ is then detected by the current transformer of the line. The fault can then be judged using (11).
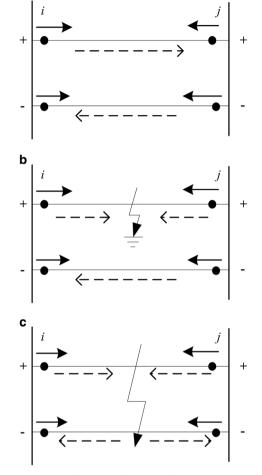
The operation state of the entire distribution system can be divided into the following three categories.

(1) Normal operation: the system has neither a fault nor power reversal. The criterion is that the fault information matrix **S** is an all-zero matrix.
(2) Fault state: the system has at least one line failure. The criteria are that **S** is a non-all-zero matrix and the current change rate of the line determined by the non-zero elements satisfies $\mathrm{d}i/\mathrm{d}t \geq 1/2b_{kc}$.
(3) Reversal of trend: the system has no fault but there are lines in the state of reversal of trend. The criteria are that **S** is a non-all-zero matrix and the current change rate of the line determined by the non-zero elements satisfies $\mathrm{d}i/\mathrm{d}t < 1/2b_{kc}$.

The matrix algorithm can judge the specific lines that may be faulty according to the current direction. The method of calculating the current increment can only judge the occurrence of the fault rather than the specific position. Therefore, the combination of the two can be more accurate.

3.4.2 Adding the function of fault-type recognition and introducing the "double D" method

If the current transformer is set only in the positive line, when a negative pole-to-ground fault appears in the system, matrix **D** will not change and the state will be mistaken for normal operation. In order to detect the failure of the negative line, the negative line network topology matrix **D'** is introduced. It is hereby stated that the positive directions of the current transformers in matrices **D** and **D'** are the same. When the system is in normal operation, the two elements in the same position in matrices **D** and **D'** are opposite of each other. Two types of fault diagrams are

Fig. 8 Fault-type diagram where the short solid arrow represents the specified current positive direction and the long dotted arrow represents the current flow. **a**: normal operation; **b** pole-to-ground fault in the positive line; **c**: pole-to-pole fault

shown in Fig. 8, where i and j represent both ends of the same line and the ends may be the power, the load, or a meeting point. The specific process to identify the fault type is described below.

(1) Normal operation, recorded as (0, 0). The two elements at the same position in matrices **D** and **D'** are opposite of each other and are non-zero. From Fig. 8a, it can be seen that $d_{ij} = 1$, $d_{ji} = -1$ in matrix **D** and $d'_{ji} = 1$, $d'_{ij} = -1$ in matrix **D'**. The criteria are that, during normal operation, d_{ij} and d_{ji} are non-zero and opposite of each other, and same for d'_{ji} and d'_{ij}.
(2) Pole-to-ground fault. Positive pole-to-ground fault and negative pole-to-ground fault are marked as (1, 0) and (0, 1), respectively. The two elements in matrix **D** or **D'** represent the current directions of the fault

occurrence line are 1 and the other elements are not affected. From Fig. 8b, it is known that $d_{ij} = d_{ji} = 1$ in matrix **D** and $d'_{ji} = 1$ and $d'_{ij} = -1$ in matrix **D'**. The criteria are that when the positive line suffers a pole-to-ground fault, $d_{ij} = d_{ji} = 1$ and d'_{ji} and d'_{ij} are opposite of each other and are non-zero. When the negative line has a pole-to-ground fault, $d_{ij} = d_{ji} = 1$ and d_{ij} and d_{ij} are opposite of each other and are non-zero.

(3) Pole-to-pole fault, recorded as (1, 1). The two elements in matrix **D** are "1" indicating that the current directions at both ends of the faulty line constitute the vertex pointing to the line and the two elements in matrix **D** 'are "– 1". From Fig. 8c, it is known that $d_{ij} = d_{ji} = 1$ in matrix **D** and $d'_{ji} = 1$, $d'_{ij} = -1$ in matrix **D'**. The criteria are: $d_{ij} = d_{ji} = 1$ and $d'_{ji} = d'_{ij} = -1$ in the faulty line.

The improved program flowchart is shown in Fig. 9 and the flowchart for determining fault type is shown in Fig. 10.

This method is applicable to online monitoring and protection system of DC distribution networks. The
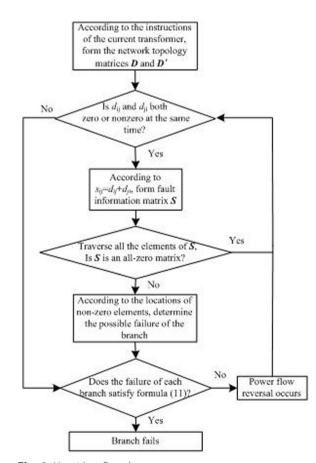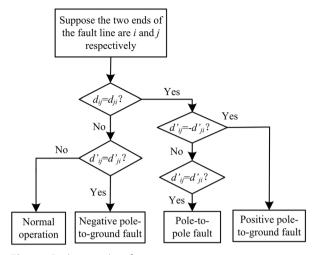

Fig. 10 Fault-type identification

algorithm first selects the lines that may be faulty in the system according to the elements in the **S** matrix and then uses the current change rate to detect the specific faulty lines. Finally, the double '**D**' method is used to detect the fault type. A further explanation for Fig. 9 is given below. Matrix **D'** is the same as matrix **D** in the second rectangular box and matrix **D** is used as an example here.

4 Results
4.1 Simulation analysis
4.1.1 Simulation system
The simulation system consists of the following six components: an AC main network, a permanent magnet direct-drive wind turbine, photovoltaic modules, a battery energy storage (BES), DC loads and AC loads. MATLAB/Simulink was used to build the model shown in Fig. 11 where the current of each current transformer on the positive line is expressed as I_{mk} (m, k refers to the current flowing from vertex m to vertex k in the specified positive direction). Similarly, the current of each current transformer on the negative line is expressed as II_{mk}. Figure 11 shows the current representation of the four current transformers between vertices 1 and 2. The simulation time is 0.2 s. A fault occurs at 0.05 s at the midpoint of the line connecting vertices 1 and 2.

G-VSC adopts double closed-loop control. The voltage control of the outer loop is droop control and the inner loop controls the current. The W-VSC operates in the maximum power point tracking mode during normal operation but in some cases requires reduced power operation. The battery operates in a charged state or as a backup power source. However, the BES unit acts as a balanced node to stabilize the DC voltage in the event of a disturbance in the main network or an island operation to
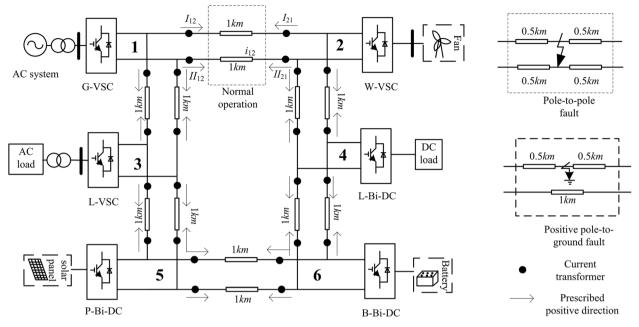

Fig. 9 Algorithm flowchart

Xu *et al. Protection and Control of Modern Power Systems* (2018) 3:27

Page 8 of 10

Fig. 11 System simulation diagram

ensure system power balance and stable operation. Photovoltaic modules are incorporated into the network through the DC-DC boost converter whose outer control adopts maximum power tracking and inner control adopts DC current control. The simulation parameters are shown in Table 1:

4.2 Simulation results analysis

Three cases, i.e. normal operation, pole-to-pole fault and positive pole-to-ground fault, were simulated and analyzed.

A. *Case study 1: Normal operation*

Table 1 Parameters of the model

DC bus voltage	500 V
Converter outlet capacitance	2 mF
Wind power unit	20 kW/220 V permanent magnet wind turbines
	Rated wind speed is 12 m/s
	Rated speed is 75 r/min
G-VSC rated power	20 kW
Battery rated power	Bi-DC rated power is 20 kW
Load unit rated power	20 kW
Line resistance	0.0139 Ω/km
Line inductance	0.159 mH/km
Line length	1 km

According to the algorithm flow, the fault information matrices S and S' for this case are given as:

$$S = \begin{bmatrix} 0 & 0 & 0 & 0 & 0 & 0 \\ 0 & 0 & 0 & 0 & 0 & 0 \\ 0 & 0 & 0 & 0 & 0 & 0 \\ 0 & 0 & 0 & 0 & 0 & 0 \\ 0 & 0 & 0 & 0 & 0 & 0 \\ 0 & 0 & 0 & 0 & 0 & 0 \end{bmatrix} S' = \begin{bmatrix} 0 & 0 & 0 & 0 & 0 & 0 \\ 0 & 0 & 0 & 0 & 0 & 0 \\ 0 & 0 & 0 & 0 & 0 & 0 \\ 0 & 0 & 0 & 0 & 0 & 0 \\ 0 & 0 & 0 & 0 & 0 & 0 \\ 0 & 0 & 0 & 0 & 0 & 0 \end{bmatrix}$$

It can be seen that both matrices are all-zero matrices and therefore, the system is judged to be in the normal operation mode.

B. *Case study 2: Pole-to-pole fault condition*

The fault information matrices S and S' for this case are given as.

$$S = \begin{bmatrix} 0 & 2 & 0 & 0 & 0 & 0 \\ 2 & 0 & 0 & 0 & 0 & 0 \\ 0 & 0 & 0 & 0 & 0 & 0 \\ 0 & 0 & 0 & 0 & 0 & 0 \\ 0 & 0 & 0 & 0 & 0 & 0 \\ 0 & 0 & 0 & 0 & 0 & 0 \end{bmatrix} S' = \begin{bmatrix} 0 & -2 & 0 & 0 & 0 & 0 \\ -2 & 0 & 0 & 0 & 0 & 0 \\ 0 & 0 & 0 & 0 & 0 & 0 \\ 0 & 0 & 0 & 0 & 0 & 0 \\ 0 & 0 & 0 & 0 & 0 & 0 \\ 0 & 0 & 0 & 0 & 0 & 0 \end{bmatrix}$$

It can be seen that the two matrices are both non-zero matrices with the non-zero elements present in S_{12} and S_{21}. It can be judged that the fault occurs in the line
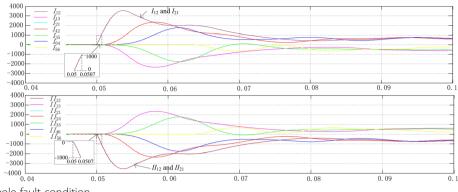
Xu et al. Protection and Control of Modern Power Systems (2018) 3:27

Page 9 of 10

Fig. 12 Pole-to-pole fault condition

between vertexes 1 and 2, and that both the positive and negative lines have faults.

To avoid misjudgment caused by power-flow reversal, the current change rate needs to be verified under the pole-to-pole fault condition. The results are shown in Fig. 12 where the fault current waveforms of the positive and negative lines are given. The change rates of fault currents I_{12} and I_{21} are both 1.43×10^6 A/s. The positive and negative fault currents are of the same magnitude but of opposite directions. The change rates of fault currents II_{12} and II_{21} are both 1.43×10^6 A/s. According to (3), the calculated value of $1/2b_{kc}$ is 1.36×10^6 A/s which satisfies (11).

It is known from the adjacency matrices D and D' that $d_{12} = 1$, $d_{21} = 1$, $d'_{12} = -1$ and $d'_{21} = -1$. According to Fig. 10, a pole-to-pole fault occurs on the line between the vertices 1 and 2.

C. Case study 3: Pole-to-ground fault condition

The fault information matrices S and S' for this case are given as:

$$S = \begin{bmatrix} 0 & 2 & 0 & 0 & 0 & 0 \\ 2 & 0 & 0 & 0 & 0 & 0 \\ 0 & 0 & 0 & 0 & 0 & 0 \\ 0 & 0 & 0 & 0 & 0 & 0 \\ 0 & 0 & 0 & 0 & 0 & 0 \\ 0 & 0 & 0 & 0 & 0 & 0 \end{bmatrix} S' = \begin{bmatrix} 0 & 0 & 0 & 0 & 0 & 0 \\ 0 & 0 & 0 & 0 & 0 & 0 \\ 0 & 0 & 0 & 0 & 0 & 0 \\ 0 & 0 & 0 & 0 & 0 & 0 \\ 0 & 0 & 0 & 0 & 0 & 0 \\ 0 & 0 & 0 & 0 & 0 & 0 \end{bmatrix}$$

It can be seen that the matrix S' is an all-zero matrix but S is a non-all-zero matrix. S_{12} and S_{21} are non-zero elements and it is possible to determine that the location of the fault is at the positive pole of the line connecting vertex 1 and vertex 2.

The current change rate needs to be verified under the pole-to-ground fault condition. The results are shown in Fig. 13 where the fault current waveforms of the positive and negative lines are given. The change rates of fault
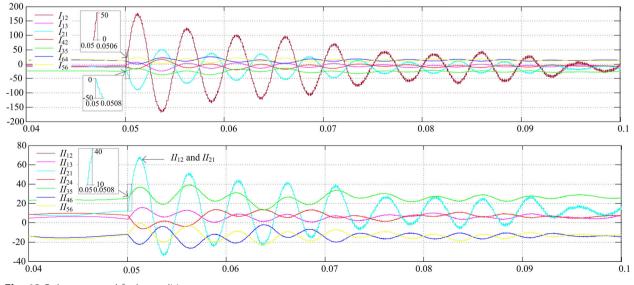

Fig. 13 Pole-to-ground fault condition

Xu *et al. Protection and Control of Modern Power Systems* (2018) 3:27

Page 10 of 10

current are 8.33×10^4 A/s and 6.25×10^4 A/s for I_{12} and I_{21}, respectively. The calculated value of $1/2b_{\text{kc}}$ according to (7) is 1.4×10^4 A/s which satisfies (11).

The adjacency matrices $\boldsymbol{D}$ and $\boldsymbol{D'}$ show that $d_{12} = 1$, $d_{21} = 1$, $d'_{12} = 0$ and $d'_{21} = 0$. Thus, according to Fig. 10, a pole-to-ground short-circuit fault is detected on the line between vertices 1 and 2.

Because the fault point is at the midpoint of the line, the parameters become symmetric. Thus, in Fig. 12, currents I_{12} and I_{21} overlap, so as currents II_{12} and II_{21}. In Fig. 13, currents II_{12} and II_{21} also coincide.

5 Conclusions
For selecting the fault line, the entire DC system is seen as a "map" by placing current transformers on both sides of the apex. The network topology matrix method and current rate of change are combined to obtain dual judgment to avoid the problem caused by no current zero crossing during a DC fault and to ensure the reliability of the detection.

For determining fault occurrence, the fault type needs to be identified. The differences between the fault information matrices are analyzed for different types of faults and the "double $\boldsymbol{D}$ method" is introduced to obtain the true validity of the method. The proposed method is suitable for a variety of topologies and fault types, and is easy to implement. Although it does require communication devices which increase the costs, with the development of DC distribution networks, communication devices will become essential from the dispatch point of view.

Availability of data and materials
Please contact author for data requests.

The innovation
This study presents methods for selecting the faulty line and identifying the fault type in a DC power distribution network, using the graph theory. The entire distribution network is considered to be a graph with the nodes represented by the vertices and connection lines represented by the edges. Current transformers help identify the current directions and current rates, which can be used for the fault-line selection and fault-type identification. Simulations verify the efficiency of the proposed methods. We believe that our study makes a significant contribution to the literature because it is easy to implement and can be applied to a large variety of devices and fault types.

Authors' contributions
XY is in charge of the conception of this article. He proposed to introduce the knowledge of graph theory into the fault line selection of DC distribution network and the structure of the whole article is controlled. LJY applied specific theoretical knowledge to the DC distribution network fault, and analyzed in detail the fault diagnosis method for different fault types, and drafted this article. FY is responsible for the simulation part of this article. All authors read and approved the final manuscript.

Authors' information
Y. Xu (1976-), male, Associate Professor, Major in new energy, power system relay protection.
J. Y. Liu (1993-), female, Master graduate student, Major in fault characteristics and protection technology of flexible DC transmission and distribution.
Y. Fu (1982-), male, lecturer, Engaged in wind power control technology research.

Competing interests
This manuscript has not been published or presented elsewhere in part or in entirety and is not under consideration by another journal. We have read and understood your journal's policies, and we believe that neither the manuscript nor the study violates any of these. The authors declare that they have no competing interests.

References
1. Jialiang, W., Rui, W., & Chang, P. (2012). Analysis of DC grid prospects in China. *Proceedings of the CSEE, 32*(13), 7–12.
2. Rabindra Mohanty, U. Sri Mukha Balaji, Ashok Kumar Pradhan, et al. (2016). "An accurate noniterative fault-location technique for low-voltage DC microgrid". *IEEE Transactions on Power Delivery, 31*(02), 475–481.
3. Monadi, M., Koch-Ciobotaru, C., Luna, A., et al. (2016). Multi-terminal medium voltage DC grids fault location and isolation. *IET Generation Transmission and Distribution, 10*(14), 3517–3528.
4. Ando, M., Schweitzer, E. O., & Baker, R. A. (1985). Development and field-data evaluation of single-end fault locator for two-terminal HVDC transmission lines-II: algorithm and evaluation. *IEEE Transactions on Power Apparatus and Systems, 104*(12), 3531–3537.
5. Dewe, M. B., Sankar, S., & Arrillaga, J. (1993). Application of satellite time references to HVDC fault location. *IEEE Transactions on Power Delivery, 8*(3), 1295–1302.
6. Zhang, X., Tai, N., Wang, Y., et al. (2017). EMTR-based fault location for DC line in VSC-MTDC system using high-frequency currents. *IET Generation Transmission and Distribution, 11*(10), 2499–2507.
7. Azizi, S., Sanaye-Pasand, M., Abedini, M., et al. (2014). A traveling-wave-based methodology for wide-area fault location in multiterminal DC systems. *IEEE Transactions on Power Delivery, 29*(6), 2552–2560.
8. Hongchun, S., Xincui, T., Guangbin, Z., et al. (2011). Fault location for ±800kV HVDC transmission lines using natural frequency of single terminal voltage data. *Proceedings of the CSEE, 31*(25), 104–111.
9. Guobing, S., XinLei, C., Gao, S., et al. (2011). Natural frequency based protection and fault location for VSC-HVDC transmission lines. *The Int Confe on Adv Power Sys Autom and Protect, 1*, 177–182.
10. Xinzhou, D., Yaozhong, G., & Bingyin, X. (1999). Research of fault location based on current traveling waves. *Proceedings of the CSEE, 19*(4), 76–80.
11. Cheng, J., Guan, M., Tang, L., et al. (2004). Paralleled multi-terminal DC transmission line fault locating method based on travelling wave. *IET Generation Transmission and Distribution, 8*(12), 2092–2101.
12. De Andrade, L., & de Leao, T. P. (2014). Fault location for transmission lines using wavelet. *IEEE Latin America Transactions, 12*(06), 1043–1048.
13. Shuping, G., Jiale, S., Guobing, S., et al. (2010). Fault location method for HVDC transmission lines on the basis of the distributed parameter model. *Proceedings of the CSEE, 30*(13), 75–80.
14. He, Z.-Y., Liao, K., Li, X.-P., et al. (2014). Natural frequency-based line fault location in HVDC lines. *IEEE Transaction on Power Delivery, 29*(2), 851–859.
15. Xinlei, C. A. I., Guobing, S. O. N. G., Shuping, G. A. O., et al. (2011). A novel fault-location method for VSC-HVDC transmission lines based on natural frequency of current. *Proceeding of the CSEE, 31*(28), 112–119.
16. Bin, L. I., & Jiawei, H. E. (2016). Research on the DC fault isolating technique in multi-terminal DC system. *Proceedings of the CSEE, 36*(1), 87–95.
17. Yang, J., Fletcher, J. E., & O'Reilly, J. (2012). Short-circuit and ground fault analyses and location in VSC-based DC network cables. *IEEE Transactions on Industrial Electronics, 59*(10), 3827–3837.
18. Helin, C., & Xu, Z. (2015). Study on transient behavior of DC flexible on-grid transmission system in offshore wind farm. *Acta Energiae Solaris Sinica, 36*(02), 430–439.
19. Fletcher SDA, Norman PJ, Galloway SJ, et al. (2012). Optimizing the roles of unit and non-unit protection methods within DC microgrids. *IEEE Transactionson Smart Grid, 3*(4), 2079–2087.